Available online at www.sciencedirect.com
SCIENCE DIRECT®
Journal of Molecular Catalysis A: Chemical 228 (2005) 125–130
JOURNAL OF MOLECULAR CATALYSIS A: CHEMICAL
www.elsevier.com/locate/molcata

Y-shaped carbon nanotubes: structural stability and transport properties

A. Latgé*, D. Grimm, P. Venezuela

Instituto de Física, Universidade Federal Fluminense, 24210-340 Niterói, RJ, Brazil

Available online 11 November 2004

Abstract

Y-shaped junctions and rings made of carbon nanotubes are proposed as possible nanostructures exhibiting quantum interference mechanisms in the electronic transport properties. The stability of the Y-structures are investigated by Monte Carlo simulations. The structures are quite stable for temperatures below 700 K. At higher temperatures, one founds a coalescence process between the two arms composing the symmetric Y-shaped rings and a formation of a localized defect in one of the arms of the asymmetric Y-shaped rings. Local electronic properties of a variety of metallic and semiconducting junction and rings are calculated by adopting a single-band tight-binding model. Remarkable changes in the electrical conductance are found by varying the length of one of the junction's arms. Interesting physical properties are investigated mainly concerned with interference processes manipulated by the sizes of the nanostructured materials.

PACS: 73.63.Fg; 73.22.−f; 73.61.Wp

Keywords: Y-shaped carbon nanotubes; Structural stability; Transport

1. Introduction

By exposing crossing single-walled carbon nanotubes (CNs) to electron beam radiation, it is possible to generate X-, T-, and Y-shaped type of junctions [1]. Alternative chemical vapor deposition processes are also developed to synthesize Y-shaped junctions (YJs) [2]. The electrical transport of those nanostructured Y-shaped systems have been investigated and it was shown to exhibit interesting rectification properties [3–5]. This fact suggests the possibility of using YJ structures as nanoscopic three-point transistors. From the mechanical point of view, sticking of the two branches of YJs under stress were predicted from molecular dynamic simulations [6]. Considering chemical aspects and taking into account that diffusion of gases through defect-free nanotubes are known to have extraordinary properties compared to other microporous materials [7], one should also expect that nanotube junctions present further interesting effects.

Under ultrasonic irradiation, pure carbon nanotubes can also fold to form nanotube rings of various diameters. Physical phenomena such as Aharonov–Bohm effects [8], magnetotransport [9], and the establishment of persistent currents [10] in those annular structures may certainly be of interest. In particular, current–voltage measurements on single carbon nanotube rings have been recently made by scanning tunneling microscopy [11]. They revealed the nanotube ring transistor properties and its potential use as building blocks for nanoscale electronic devices.

We have recently proposed the realization of ring-like structures made of two coupled carbon nanotube Y-junctions [12]. Those YJ-ring systems may act as a double-slit-like electron interferometer, with conductance exhibiting strong oscillations as functions of energy and arm lengths. Here, we extend our investigations of electronic and transport properties on Y-shaped structures, adopting single-band tight-binding calculations within the Green function formalism. Conductance as functions of the Fermi energy and characteristics sizes of the structures are studied using the Landauer–Kubo formalism. We also investigate the structural stability of the theoretical proposed Y-shaped tubes and rings. Monte Carlo (MC) numerical simulations are performed by adopting an interatomic potential proposed by Tersoff [13] and considering periodic boundary conditions. Averaged binding

* Corresponding author. Tel.: +55 21 2629 5812; fax: +55 21 2629 5878.
E-mail address: latge@if.uff.br (A. Latgé).

1381-1169/$ – see front matter © 2004 Elsevier B.V. All rights reserved.
doi:10.1016/j.molcata.2004.09.063

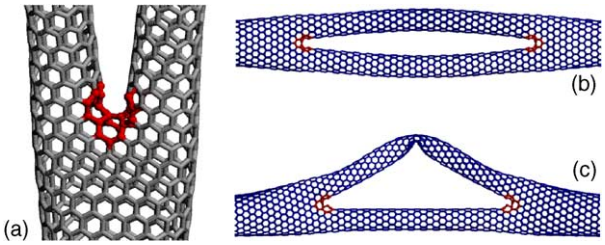

Fig. 1. (a) Equilibrium atomic configurations of a 18 → 9/9 YJ. A symmetric and an asymmetric YJ-rings are depicted in (b) and (c), considering equal and different arm lengths, respectively. The topological defects composed of six heptagons are shown by dark atoms.

energies and formation energies of the Y-ring structures are presented as a function of temperature. In what follows, we restrict our study to zigzag achiral tubes (n, 0) that may act as semiconducting and metallic systems depending upon the corresponding chiral n integer number.

Three examples of equilibrium atomic configurations are shown in Fig. 1: a YJ and two kinds of YJ-rings, called in what follows as symmetric and asymmetric, depending upon the equivalence between the lengths of the two arms composing the ring, respectively. These structures are made out of (18, 0)–(9, 0)/(9, 0) YJs [named here as 18 → 9/9], where the (18, 0) tube corresponds to a zigzag CN lead that bifurcates into two (9, 0) CN arms. A topological defect, composed of six heptagons, induces the bifurcation, in accordance with the Crespi rule [14]. The heptagons (dark colors) are localized exactly at the junction centers. Notice that in these particular examples all three constituent tubes are metallic-like CNs.

In the ring shown in Fig. 1(b), both lengths of the (9, 0) CN arms measure $54a_{cc}$, whereas the asymmetric ring shown in Fig. 1(c) exhibits two different arm lengths, measuring $54a_{cc}$ and $42a_{cc}$, a_{cc} being the carbon–carbon atomic distance in graphite. Our simulation results unequivocally show that those ring-like systems are structurally stable and, in principle, may be realized experimentally. One possibility would be by using CN coalescence under electron irradiation, via a zipper-like mechanism [15,16].

2. Structural stability

To study the structural stability of the Y-shaped structures, we performed MC numerical simulations, adopting the interatomic potential proposed by Tersoff [13]. One should point out that the Tersoff potential has been successfully used to reproduce elastic properties and defect energies of carbon-based materials such as graphite and diamond, and more recently is being extensively adopted in the description of carbon nanotubes [15]. The MC simulations are performed in the isothermal–isobaric ensemble, where the number of particles, temperature and pressure are kept constant. All the simulations presented here are performed at zero pressure; due to periodic boundary conditions, the lengths of the junctions can vary during the simulations.

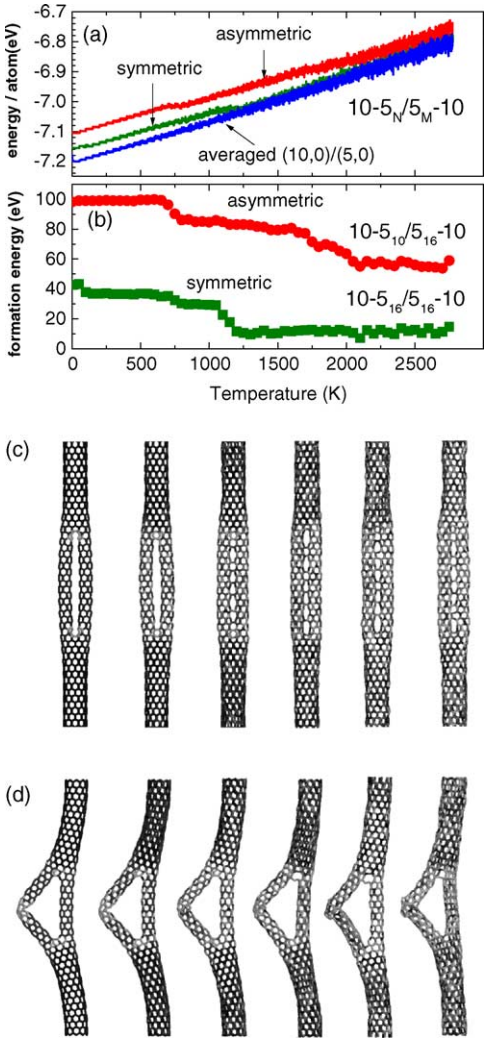

Fig. 2. (a) Average energy per atom and (b) formation energy as a function of temperature of 10 → 5/5 → 10 YJ-rings. Green-colored curves (on-line) correspond to symmetric, red-colored ones (on-line) to asymmetric YJ-rings, and the blue one gives the corresponding result of the averaged pristine nanotube counterparts [(5, 0)/(10, 0)]. Atomic configurations of the symmetric and asymmetric YJ-rings are shown in (c) and (d), respectively, corresponding to temperatures of 0, 500, . . . , 2500 K, from left to right. The atoms are represented in a gray scale where brighter colors indicate higher atom energies.

Our goal is to study the thermal stability of YJ-rings. After the simulation reaches equilibrium at 0 K, the temperature is increased by consecutive steps of 50 K maintaining the system in quasi-equilibrium states. At each step, the system is completely relaxed. Numerical simulations until $T = 3000$ K for 10 → 5/5 → 10 YJ-rings and the corresponding pristine nanotube counterparts (5, 0) and (10, 0) are presented in Fig. 2.

The average energy per atom and the structural formation energy as a function of temperature, are shown in Fig. 2(a) and (b), respectively. The energy results for symmetric (arms measuring $24a_{cc}$) and asymmetric ($15a_{cc}$ and $24a_{cc}$) YJ-rings are compared with each other and also with a corresponding averaged straight composed (5, 0)/(10, 0) CN. As ex-

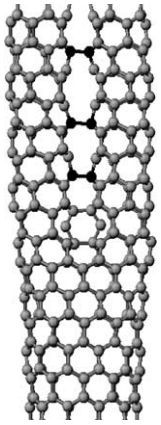

Fig. 3. Close-up of the atomic configuration for the symmetric YJ-ring of Fig. 2(c) at 1000 K.

pected, the average energy per atom increases with temperature for all considered systems whereas the formation energy decreases with temperature. The existence of energy plateaus indicates temperature ranges without major structural changes. More important, at the first plateau (for temperatures below ≈700 K), there are no structural changes, unless thermal atomic vibrations, compared to the proposed original configuration used in the transport calculations. This can be verified in Fig. 2(c) and (d), where the atomic configurations at different temperatures are presented in gray scale with brighter colors indicating higher atomic energies. In Fig. 2(d), we observe that the asymmetric YJ-ring forms a localized kink-defect in the middle of the bigger arm. It is interesting to note [see Fig. 2(b)] that the formation energies of the symmetric YJ-ring are always smaller than those of the asymmetric one, due to the energy cost of the observed kink formation. It means, as expected, that symmetric YJ-rings are more likely to be formed than asymmetric ones. On the other hand, a polymerization process, between the arms of the symmetric YJ-ring is evident as the temperature increases, as shown in Fig. 2(c). These structural changes occur for temperatures above a critical value of ≈700 K. In Fig. 3, a close-up of the polymerized symmetric YJ-ring (for $T =$ 1000 K) is shown. The black balls represent four-fold coordinated carbon atoms which bind during the polymerization process.

For higher temperatures, the polymerized arms of the symmetric YJ-ring will eventually coalesce. Fig. 4(a) exhibits the atomic configuration of a YJR at 5000 K. Cooling the ring down to 0 K, the atoms of the former ring arms are rearranged and the system forms a nearly defect-free single-walled (10, 0) CN as depicted at in Fig. 4(b). A similar coalescence process has been recently observed during electron irradiation of CN bundles [15].

Preliminary results with YJ-ring composed of CNs with larger diameters indicate much lower formation energies and a structural stability up to quite higher temperatures. As the Tersoff potential is a short-ranged one and does not include van der Waals interactions (which tend to maintain parallel

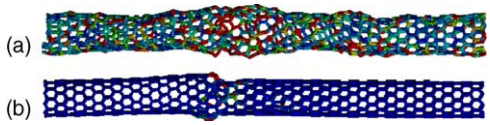

Fig. 4. Coalescence process of the arms of a symmetric YJ-ring: (a) heated to 5000 K and (b) cooled down to 0 K, where a nearly pristine (10, 0) CN configuration is obtained. Brighter colors indicate higher atomic energies.

tubes in bundles at a distance of ≈3.4 Å), a significant up shift of the critical temperatures of symmetric YJ-rings is expected.

3. Electronic and transport properties

The electrical properties of CN systems are studied by using a single π-band tight-binding model [17]. The Hamiltonian is written in the site representation, as a sum over all m lattice sites as

$$\mathbb{H} = \sum_{m \neq n} t_{mn} \mathbf{a}_m^\dagger \mathbf{a}_n, \tag{1}$$

in terms of the electronic creation $\mathbf{a}^\dagger$ and annihilation $\mathbf{a}$ operators. The on-site energies are given by $t_{mm} = e_0$ while the hopping integrals t_{mn} are restricted to first neighbor sites and considered equal to γ_0 (≈−2.66 eV). Using the Green function formalism, one defines G as the solution of the inhomogeneous differential equation [18]

$$G(\omega) = (\omega - \mathbb{H})^{-1}, \tag{2}$$

with ω being a complex energy variable. The poles of the Green function define the eigenvalues ϵ of the Hamiltonian. To assure the non-divergence of the Green function over the whole real axis range, a small imaginary part is added, i.e., $\omega = \epsilon \pm \eta$. Physically one may think that a finite η value introduces a relaxation time due to electronic scattering mechanisms.

The zigzag tubes used here to form the Y-shaped structures are theoretically described by considering a chain of rings disposed along the tubular axial direction as displayed in Fig. 5(a). Each ring includes the two carbon atoms associated with the non-equivalent sites of the graphene unit cell, and is connected to two other adjacent rings via two different hopping matrices [see Fig. 5(b)] named $V_{01} = V_{10} = V_1$ (joining even numbered atoms) and $V_{0\bar{1}} = V_{\bar{1}0} = V_2$ (odd atoms). All the Green functions are calculated in real space by using renormalization techniques and are obtained by the matricial Dyson's relation [19,20]

$$G_{ij} = G_{ij}^0 \delta_{ij} + \sum_k G_{ii}^0 V_{ik} G_{kj}, \tag{3}$$

with G_{ij}^0 being the uncoupled propagator. The renormalization procedure starts by coupling rings 0, 1, and $\bar{1}$, for exam-

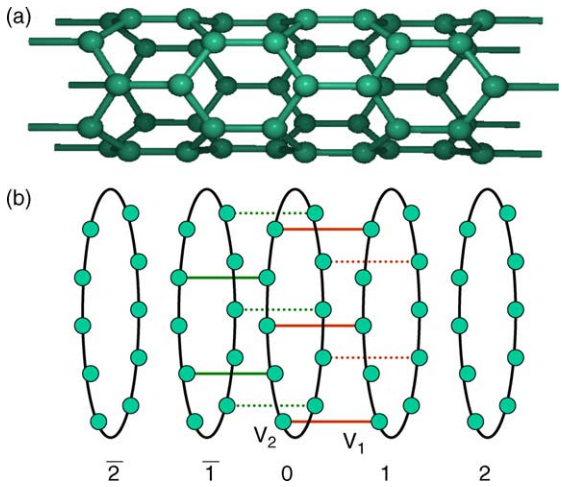

Fig. 5. Schematic representation of (a) a zigzag CN and (b) the quasi-one-dimensional description of the CN, with the two hopping matrices, V_1 and V_2, marking explicitly the interactions between alternated carbon sites disposed along the rings.

ple, to their two first neighbor rings, respectively, resulting in

$$\begin{aligned} G_{00} &= g + gV_{01}G_{10} + gV_{0\bar{1}}G_{\bar{1}0}, \\ G_{10} &= gV_{10}G_{00} + gV_{12}G_{20}, \\ G_{\bar{1}0} &= gV_{\bar{1}0}G_{00} + gV_{\bar{1}\bar{2}}G_{\bar{2}0}, \end{aligned} \tag{4}$$

where g is the dressed renormalized Green function of the ring-cell, given by $g = (I - g_0V_{00})^{-1}g_0$, with I being the identical matrix and g_0 a diagonal matrix with elements given by $1/(\omega - e_0)$. We use the fact that in pristine achiral CNs, all cells are taken as equal. The dressed locator after this first step is written in terms of second neighbor rings, and so on.

After $N + 1$ recurrence steps, one obtains [19,20]

$$\begin{aligned} g^{(N+1)} &= [1 - Z_1^{(N)}(1 - Z_2^{(N)}Z_2^{(N)})^{-1}Z_1^{(N)}Z_1^{(N)} \\ &\quad - Z_2^{(N)}(1 - Z_1^{(N)}Z_1^{(N)})^{-1}Z_2^{(N)}Z_2^{(N)}]^{-1}g^{(N)}, \\ V_{1,2}^{(N+1)} &= V_{1,2}^{(N)}(1 - Z_{2,1}^{(N)}Z_{2,1}^{(N)})^{-1}Z_{2,1}^{(N)}Z_{1,2}^{(N)}, \end{aligned} \tag{5}$$

where $Z_i^{(N)} = g^{(N)}V_i^{(N)}$. As $N \to \infty$, the process converges to a fix point $g^{(N)} = G^*$, since $V_i^{(N)} \to 0$. The local density of state can be directly obtained from this dressed-renormalized Green function by $\rho(\epsilon) = \mp\frac{1}{\pi}\mathrm{Im}(\mathrm{Tr}\, G^{\pm}(\epsilon))$, where the trace is taken over the cell atomic sites.

Electrical transport properties of CNs, YJs and YJ-rings are investigated by using the Landauer–Kubo formalism [21,22]. Within the linear regime, the conductance of the system is proportional to the current flux between two adjacent cells i and j (labeled 0 and 1). At zero temperature, it may be given as

$$\Gamma(E) = \frac{4e^2}{h}\mathrm{Tr}\sum_{mnlk=0,1}(-1)^{n+k}V_{mn}G_{nk}^I(E)V_{kl}G_{lm}^I(E), \tag{6}$$

where $G_{mn}^I(E)$ denotes the imaginary part of the retarded one-electron propagator matrix. One should note that all microscopic details are intrinsically included in this real space picture and the atomic arrangement of the topological defects presented at the junctions are properly taken into account, with no need of further approximations.

Local density of states (LDOS) and conductance as functions of energies of YJ junctions composed of mixture of semiconducting and metallic branches have been discussed, considering junctions formed by three infinite legs. Interestingly, depending on the composition of the YJ, one may determine the size of the transport gap via the conductance results, that are not always coincident with the results of the corresponding averaged density of states. In particular, when the main branch is a semiconductor tube which bifurcates into a metallic and smaller semiconducting nanotubes, the averaged local density of states presents contributions from the extended metallic states which populate the semiconducting energy gap [12]. Also, a YJ formed with a finite leg may be thought as a control terminal which regulates the electronic transport along the structure.

The electronic and transport properties of the proposed ring-like structure may be discussed first on the basis of an equivalent one-dimensional counterpart structure composed of a single loop with two semi-infinite chains (leads) attached at opposite sites. Results for the conductance of such an example of one-dimensional ring, composed of equal number of atoms on both branches of the loop (symmetric ring) are depicted in Fig. 6(a). In what follows all energies results are given in units of the nearest neighbor hopping integral γ_0.

All the results exhibit a well defined oscillation pattern with the corresponding periods being driven by the inverse of the branch size. One should note that, independently of the size of the symmetric loop, the conductance is not completely destroyed as a consequence of the constructive superposition of the electronic wave functions along the two equal quantum paths. Similar results for an asymmetric ring are obtained [see Fig. 6(b)] except that in that case destructive quantum interferences are manifested in zero conductance due to the different length size of the branches. One may also point out that localized states appear at the LDOS of both symmetric and asymmetric rings [not shown in the figure] which are reminiscences of strictly one-dimensional loops (without the attached semi-infinite chains). A summary of the results of quantum interference effects on the transport along the Y-shaped rings are presented in Fig. 6(c) which shows the conductance minima values for different combinations of arm lengths in the one-dimensional rings.

The same general conclusions are also addressed in the YJ-ring case as it is clearly shown in Fig. 6(d) and (e) for metallic CN YJ-rings such as $12 \to 6_N/6_M \to 12$ with N and M being the number of rings of the two YJ-ring paths. Quantum interference phenomena related to the symmetric ($N = M$) and asymmetric ($N \neq M$) configurations are also presented within the energy range for which a pure metallic (12, 0) CN exhibits two ballistic channels. The minima con-

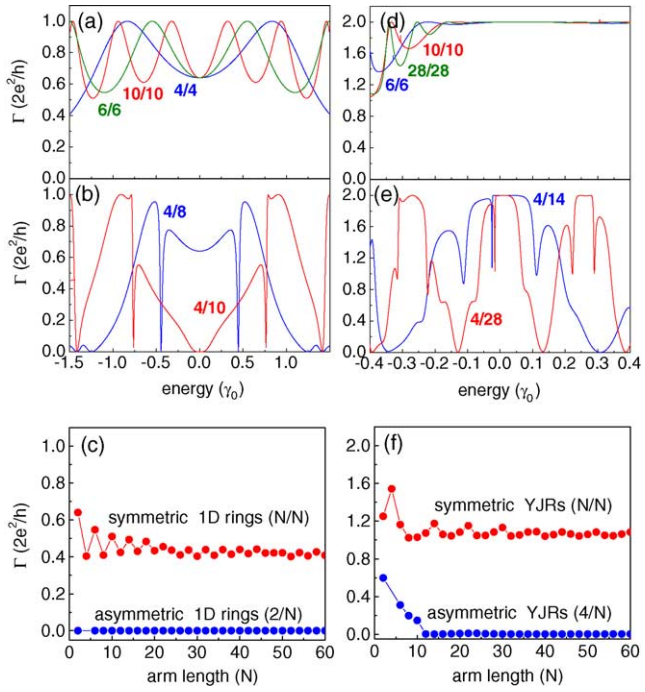

Fig. 6. Conductance dependence on the Fermi energy for the one-dimensional ring model in (a) and (b) and for $12 \rightarrow 6_N/6_M \rightarrow 12$ YJ-rings in (d) and (e), considering symmetric ($N = M$) and asymmetric ($N \neq M$) arm configurations, respectively. Panels (c) and (f) show the minimum values for the conductance of both configurations for the one-dimensional ring description and the YJ-rings studied, as a function of the length of one of the arms.

ductance is always found to be zero in the asymmetric case, beyond a certain difference between the sizes of the two arms composing the ring, as it is shown in Fig. 6(f). This is a clear evidence of destructive quantum interference effects associated with the two distinct CN paths that the electrons may take as they travel across the YJ-ring structure. In contrast, for symmetric YJ-rings the minimum conductance value is always greater than one unit channel, independently of the arm length and no general transport suppression is observed.

To explore further aspects of the interference phenomena in the transport of YJ-rings, we discuss the case of a semiconductor ring with metallic main branches on both sides of the junction, i.e., we analyze the ring $12 \rightarrow 5_N/7_M \rightarrow 12$. The results for the conductance as a function of the Fermi level are depicted in Fig. 7. As expected, due to the transport barrier imposed by the finite semiconducting ring, the conductance is reduced but does not go to zero at the Fermi level if the arm sizes are not bigger than the extension of the wave function corresponding to the metallic main path. A detailed analysis of the conductance dependence on the sizes of the loop evidences that the transport is completely blockaded when the lengths overcome a critical value.

Other interesting investigation on the manifestation or not of interference aspects on the electronic transport proposed here may be further performed and we believe that they are quite relevant for a better understanding of the variety of possibilities presented when forming molecular carbon-based complexes composed of individual tubes. An important result of the present work is the determination of a structural stability for a large range of temperature for the Y-junction and Y-shaped ring proposed. Of course, one may stress the important role in determining transport properties, played by the metallic contacts which are described in our model by single tubes composing the main junction branches. We believe also that even by adopting simple electronic model such as the single π-band used here, we are able to discuss the main effects of geometric aspects on quantum phenomena that essentially regulate electronic transport responses. We may also incorporate in the theoretical description other kinds of external perturbation such as pressure and external electric and magnetic fields on the junction systems proposed. In that sense, we are able to propose their use as electronic devices which has been a great motivation in molecular nanoscience and nanotechnology nowadays.

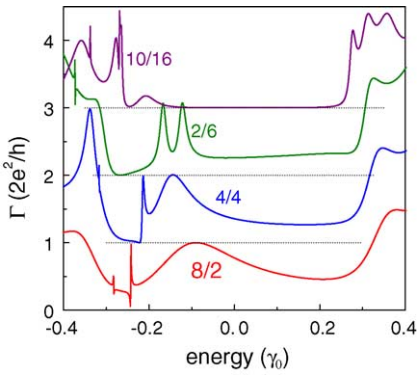

Fig. 7. Conductance as a function of the Fermi energy of $12 \rightarrow 5_N/7_M \rightarrow 12$ YJ-rings, simulating semiconducting rings with metallic contacts made of (12, 0) tubes. The curves corresponding to different combinations of arm lengths given by the integer pair N/M are shifted upwards.

Acknowledgments

This work was partially supported by the Brazilian Agencies CNPq, CAPES, FAPERJ, and Instituto do Milênio para Nanociências/MCT.

References

[1] M. Terrones, F. Banhart, N. Grobert, J.-C. Charlier, H. Terrones, P.M. Ajayan, Phys. Rev. Lett. 89 (2002) 75505.
[2] C. Papadopoulos, A. Rakitin, J. Li, A.S. Vedeneev, J.M. Xu, Phys. Rev. Lett. 85 (2000) 3476.
[3] L.P. Biró, R. Ehlich, Z. Osváth, A. Koós, Z.E. Horváth, J. Gyulai, J.B. Nagy, Diamond Relat. Mater. 11 (2002) 1081.
[4] A. Andriotis, M. Menon, D. Srivastava, L. Chernozatonskii, Phys. Rev. B 65 (2002) 165416.
[5] V. Meunier, M.B. Nardelli, J. Bernholc, T. Zacharia, J.-C. Charlier, Appl. Phys. Lett. 81 (2002) 5234.
[6] L.A. Chernozatonskii, I.V. Ponomareva, JETP Lett. 78 (2003) 327.
[7] A.I. Skoulidas, D.M. Ackerman, J.K. Johnson, D.S. Sholl, Phys. Rev. Lett. 89 (2002) 185901.

[8] L.A. Chernozatonskii, Phys. Lett. A 172 (1992) 173.
[9] R. Martel, H.R. Shea, Ph. Avouris, Nature 398 (1999) 299;
H.R. Shea, R. Martel, Ph. Avouris, Phys. Rev. B 58 (1998) 12671;
H.R. Shea, R. Martel, Ph. Avouris, Phys. Rev. Lett. 84 (2000) 4441.
[10] S. Latil, S. Roche, A. Rubio, Phys. Rev. B 67 (2003) 165420.
[11] H. Watanabe, C. Manabe, T. Shigematsu, M. Shimizu, Appl. Phys. Lett. 78 (2001) 2928.
[12] D. Grimm, R.B. Muniz, A. Latgé, Phys. Rev. B 68 (2003) 193407.
[13] J. Tersoff, Phys. Rev. Lett. 61 (1988) 2879;
J. Tersoff, Phys. Rev. B 37 (1988) 6991.
[14] V.H. Crespi, Phys. Rev. B 58 (1998) 12671.
[15] M. Terrones, H. Terrones, F. Banhart, J.-C. Charlier, P.M. Ajayan, Science 288 (2000) 1226.
[16] M. Yoon, et al., Phys. Rev. Lett. 92 (2004) 75504.
[17] R. Saito, G. Dresselhaus, M.S. Dresselhaus, Physical Properties of Carbon Nanotubes, Imperial College Press, 1998.
[18] E.N. Economou, Green's Functions in Quantum Physics, second ed., Springer-Verlag, Berlin, 1983.
[19] M.S. Ferreira, T.G. Dargam, R.B. Muniz, A. Latgé, Phys. Rev. B 62 (2000) 16040;
M.S. Ferreira, T.G. Dargam, R.B. Muniz, A. Latgé, Phys. Rev. B 63 (2001) 245111.
[20] C.G. Rocha, T.G. Dargam, A. Latgé, Phys. Rev. B 65 (2002) 165431.
[21] R. Kubo, J. Phys. Soc. Jpn. 12 (1957) 570.
[22] J. Mathon, M. Villeret, H. Itoh, Phys. Rev. B 52 (1995) R6983.